8-15-2002

Water Confined in Cylindrical Micropores

Robert W. Thompson
Worcester Polytechnic Institute, rwt@wpi.edu

Arjan Giaya
Worcester Polytechnic Institute

Water confined in cylindrical micropores

Arjan Giaya and Robert W. Thompson[a)]
Department of Chemical Engineering, Worcester Polytechnic Institute, Worcester, Massachusetts 01609

(Received 11 October 2001; accepted 24 May 2002)

A model characterizing water-like fluids confined in cylindrical micropores is presented. The equation of state was derived based on perturbation theory assuming that the reference system of hard spheres confined in the cylindrical pores is homogenous. The perturbed state accounts for fluid–fluid, fluid–wall, and hydrogen bonding interactions. Fluid–fluid and fluid–wall interactions are modeled as the pairwise sum of Lennard-Jones potentials. The hydrogen bonding model accounts for the open structure of liquid water, as well as for the fact that the hydrogen bonding capabilities of confined molecules are distorted. This model was used to analyze the dependence of the density of water inside the micropores on the density outside the pores, the pore radius, and the affinity of the pore walls for water molecules. For gas-phase adsorption, the model predicts that the density of water inside the pores depends on the fluid–wall interactions. The state of the adsorbed phase varies from the density of vapor outside the pores (for the hard sphere wall) to a bulk liquid-like density (for a hydrophilic sample). The predicted behavior of confined water in the presence of bulk liquid outside the pores was more interesting. The model predicts that for small pores of hydrophobic materials, the density of fluid inside the pores is much smaller than the bulk liquid density, i.e., vapor-like. However, as the radius and/or hydrophility are increased, the fluid density inside the pores approaches the bulk liquid density very rapidly. © *2002 American Institute of Physics.* [DOI: 10.1063/1.1494419]

I. INTRODUCTION

Microporous and mesoporous materials are often of interest in water and (humid) gas treatment. Recently, Giaya *et al.*[1] studied the adsorption of chlorinated volatile organic compounds (CVOCs) on a silicalite and a dealuminated Y (DAY) zeolite sample. Silicalite has pore openings of about 5.5 Å. Zeolite Y has pore openings of about 7.5 Å into cages of about 13 Å diameter. Details about these specific samples can be found in Ref. 1. Giaya *et al.*[1] found that silicalite had a much better adsorption capacity compared to DAY, although the latter was slightly more hydrophobic (as shown by water temperature desorption measurements). Initially, it was thought that silicalite might have inherently higher affinity for these organics. However, as reported in Giaya and Thompson,[2] adsorption studies from the pure gas phase revealed that both materials, silicalite and DAY, had high affinities for CVOCs. Also, pure water temperature desorption data and pure gas phase CVOC adsorption data showed that DAY was as hydrophobic as silicalite, if not more so. Yet, the adsorption of the same CVOCs out of liquid water showed silicalite had superior adsorption capacity when compared with DAY. These differences might be explained in terms of different phases of water confined in the pores of these materials.

It was suggested earlier[1] that liquid water may ''penetrate'' the pores of silicalite, but not pores of DAY. To check this suggestion two approaches were taken. First, apparent and true densities were measured experimentally by water and CVOC displacement methods. By looking at these data one might gather some information about the ability of water liquid to form inside the pores of these materials. Second, we attempted to predict the density of the water phase inside the pores of silicalite and DAY theoretically, using relationships describing the thermodynamic properties of confined water.

II. TRUE AND APPARENT SOLID DENSITY VALUES

Based on CVOC adsorption experiments, Giaya *et al.*[1] have suggested that water does not enter the pores of highly hydrophobic silicalite. Whether pores are accessible by liquid water or not can be verified by comparing the true and effective densities.

Following Brunauer, Emmett, and Teller (BET) (in Gregg and Sing[3]), the true density is given as the mass of the solid divided by the volume of the solid excluding open and closed pores. The effective solid density is determined by a given liquid displacement method. Here for analogy, the true volume means the volume of the solid (excluding open and closed pores); the effective volume is the volume occupied by solid and its pores as determined by a liquid displacement method.

If the volume of silicalite determined by the water displacement method differs from silicalite true volume by the specific pore volume, then one can safely say that the liquid water does not enter the silicalite pores.

The specific effective volume values for silicalite and dealuminated Y (DAY) samples were determined by water and trichloroethylene (TCE) displacement methods. The results, given in Table I, showed that the specific volume of

[a)]Electronic mail: rwt@wpi.edu

TABLE I. Specific volumes determined by water and TCE displacement method.

	Silicalite	DAY[a]	CAC[b]
Specific volume by H_2O, $V_{H_2O}(cm^3/g)$	0.549	0.472	0.583
Specific volume by TCE, $V_{TCE}(cm^3/g)$	0.449	0.491	0.553
$(V_{H_2O}-V_{TCE})(cm^3/g)$	0.100	−0.019	0.030
Pore volume determined by N_2 adsorption, $V_t(cm^3/g)$	0.21	0.38	0.51

[a]Dealuminated zeolite NaY obtained from Zeolyst.
[b]Centaur® granular activated carbon obtained from Calgon.

silicalite determined by water displacement was very different from the specific volume determined by TCE displacement. The difference between those two values was 0.100 cm^3/g while the total micropore volume for silicalite is 0.19 cm^3/g, measured by BET nitrogen adsorption. Unlike silicalite, the difference in effective specific volumes for the DAY sample was almost insignificant, −0.019 cm^3/g, compared to its BET pore volume of 0.38 cm^3/g. Insignificant differences also were observed for the activated carbon sample. These data show that a dense, liquid-like water phase can be formed inside the pores of the DAY and GAC samples. However, about half of the void volume of silicalite is accessible to liquid-like water.

III. MODEL DEVELOPMENT

Molecular dynamics and Monte Carlo simulations are often used for theoretical studies of confined fluids.[4] These methods are perhaps most exacting, but also most computationally intensive. On the other hand, methods that involve the mean-field approximation are less exact, but also less computationally demanding. Diestler and Schoen,[5] and more recently, Schoen and Diestler[6] and Truskett *et al.*[7] studied the behavior of confined fluid based on the mean-field theory. Schoen and Diestler[6] studied the thermodynamic behavior of a nonassociating fluid confined to a slit pore, applying the perturbation theory. Truskett *et al.*[7] extended that approach to include fluid–fluid hydrogen bonding interactions.

From previous works[5–7] the Helmholtz free energy is given by

$$F=-\beta^{-1}\ln\frac{Z_N^{(0)}}{N!\Lambda^{3N}}+\langle U_{fw}^{disp}\rangle_0+\langle U_{ff}^{disp}\rangle_0+\langle U_{ff}^{HB}\rangle_0, \quad (1)$$

where $Z_N^{(0)}$ is the configurational partition function for the confined hard sphere fluid, and $\langle U_{fw}^{disp}\rangle_0$, $\langle U_{ff}^{disp}\rangle_0$, and $\langle U_{ff}^{HB}\rangle_0$ are potential energies of, respectively, fluid–wall, fluid–fluid, and hydrogen bonding interactions, averaged over the unperturbed probability distribution.

Equation (1) is a general expression for the Helmholtz free energy, F, of a confined fluid, independent of the pore geometry. Schoen and Diestler[6] evaluated each term of Eq. (1) (except the hydrogen bonding term) for a simple fluid confined in a slit-type pore. Truskett *et al.*[7] extended that model for an associating fluid confined in slit-type pore as well. They treated water molecules as uniform spheres when evaluating the repulsive and dispersive interactions, since those interactions were expected to play a minor role in the structuring of fluid molecules.[7] The same approach is taken in this work and applied for cylindrical geometry. The orientational dependent hydrogen bonding model is based on Truskett *et al.*,[7,8] which was recently refined by Giaya and Thompson.[9] In the following sections each term of Eq. (1) is evaluated for the case of water in a cylindrical pore.

Some conditions for our system are: the pore is infinitely long, the diameter of a fluid molecule is σ_f, whereas that of a pore (wall) molecule is σ_w, the radius of the cylinder accessible to fluid molecules is R. The wall thickness is taken to be infinite, N is the number of spherical fluid molecules contained in the cylindrical volume with height H.

Following Truskett *et al.*[7] and Schoen and Diestler,[6] the exact differential of the Helmholtz free energy for the fluid confined in cylindrical pores can be expressed as:

$$dF=d(U-TS)=-S\,dT-\pi R^2P_{\|}dH+\mu\,dN, \quad (2)$$

where S is the entropy, T is the temperature, $P_{\|}$ is the pressure along the pore axis, and μ is the chemical potential.

A. Energy of the reference system

A hard sphere fluid confined in a hard sphere cylindrical wall is taken as a reference system, in analogy with previous works.[5–8] Moreover, the wall is considered to be smooth, that is, ignoring local variations on the wall surface. First, we define the energy of the reference system $U^{(0)}$. Thus,

$$U^{(0)}=\tfrac{1}{2}\sum_{i=1}^{N}\sum_{j\neq i}^{N}u_{ff}^{HS}(r_{ij})+\sum_{i=1}^{N}u_{fw}^{HS}(r_i), \quad (3)$$

where r_{ij} is the distance between two spherical fluid molecules positioned at r_i and r_j,

$$u_{ff}^{HS}(r_{ij})=\begin{cases}0, & r_{ij}>\sigma_f\\ \infty, & r_{ij}\leqslant\sigma_f,\end{cases} \quad (4)$$

and

$$u_{fw}^{HS}(r_i)=\begin{cases}0, & r_i<R-\sigma_f/2\\ \infty, & r_i\geqslant R-\sigma_f/2.\end{cases} \quad (5)$$

The configurational integral of the reference system is approximated as[6]

$$Z_N^{(0)}=[Z_1^{(0)}]^N, \quad (6)$$

where $Z_1^{(0)}$ is the effective single molecule, assumed to be equal to the volume accessible to any given molecule.[6] Therefore, for the cylindrical pore:

$$Z_1^{(0)}=\pi R^2H-Nb_p(R), \quad (7)$$

$b_p(R)$ is the van der Waals excluded volume parameter, which for a confined fluid is defined[7] as

$$b_p(R)=\frac{1}{\rho_p[\,\eta_p=0.64]}, \quad (8)$$

where $\rho_p[\,\eta_p=0.64]$ is the pore density at which the mean packing fraction η_p in the pore attains the value $\eta_p=0.64$. The relation between η_p and ρ_p is derived in Appendix B

[see Eq. (B6)]. As R goes to infinity, the value of $b_p(R)$ equals the van der Waals excluded volume parameter of the bulk fluid, defined as[8]

$$b_b=\frac{\pi\sigma_f^3}{6\times 0.64}. \tag{9}$$

Then

$$Z_N^{(0)}=(\pi R^2 H-Nb_p(R))^N. \tag{10}$$

For a homogeneous fluid,

$$\rho_0(r_i)=\rho_p=\frac{N}{\pi R^2 H}. \tag{11}$$

Then

$$Z_N^{(0)}=N^N\left(\frac{1-\rho_p b_p(R)}{\rho_p}\right)^N. \tag{12}$$

B. Fluid–wall potential

The averaged fluid–wall potential is denoted as $\langle U_{\mathrm{fw}}^{\mathrm{disp}}\rangle_0$. Let $U_{\mathrm{fw}}^{\mathrm{disp}}(r_i)$ represent the potential of a molecule in distance r_i from the z axis of the cylindrical pore. (The fluid–wall potential depends only on r_i, since the wall is assumed to be molecularly smooth.) This potential is calculated based on the Lennard-Jones attraction between a fluid molecule and a molecule in the solid volume. The derivation of this equation is shown in Appendix A:

$$U_{\mathrm{fw}}^{\mathrm{disp}}(r_i)=-\pi\rho_s\epsilon_{\mathrm{fw}}\sigma_{\mathrm{fw}}^6 I_{\mathrm{fw}}, \tag{13}$$

where ρ_s is the density of wall molecules, ϵ_{fw} is the Lennard-Jones potential parameter for the fluid–wall interaction, and I_{fw} is the integral given by

$$I_{\mathrm{fw}}=\int_0^{\pi}\frac{d\phi}{[\sqrt{(R+\sigma_{\mathrm{fw}})^2-r_i^2\sin^2\phi}-r_i\cos\phi]^3}. \tag{14}$$

The average fluid–wall potential for the cylindrical volume with height H is

$$\langle U_{\mathrm{fw}}^{\mathrm{disp}}\rangle_0=\int_V dr_i\,\rho_0(r_i)U_{\mathrm{fw}}^{\mathrm{disp}}(r_i), \tag{15}$$

where $\rho_0(r_i)$ is the local density at point r_i, which for a homogenous fluid is simply ρ_p. The integral for $\langle U_{\mathrm{fw}}^{\mathrm{disp}}\rangle_0$ can be transformed as follows:

$$\begin{aligned}\langle U_{\mathrm{fw}}^{\mathrm{disp}}\rangle_0&=\rho_p\int_0^H dh\int_0^{2\pi}d\theta\int_0^R dr_i\,r_i U_{\mathrm{fw}}^{\mathrm{disp}}(r_i)\\&=2H\pi\rho_p\int_0^R dr_i\,r_i U_{\mathrm{fw}}^{\mathrm{disp}}(r_i).\end{aligned} \tag{16}$$

Substituting in Eqs. (11), (13), (14), and after some transformations, we can get

$$\langle U_{\mathrm{fw}}^{\mathrm{disp}}\rangle_0=\epsilon_{\mathrm{fw}}N\Psi(R)=N\Psi_p(R), \tag{17}$$

where

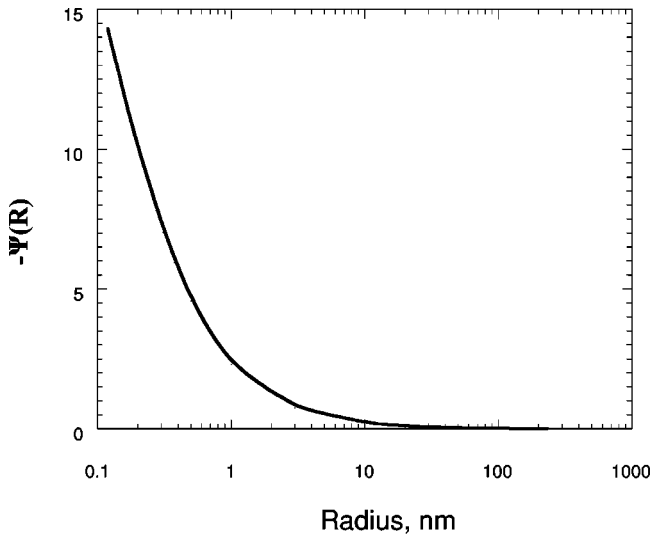

FIG. 1. The influence of the fluid–wall interactions as a function of the pore radius. $\Psi(R)$ is defined by Eq. (18).

$$\begin{aligned}\Psi(R)=&-2\pi\rho_s\sigma_{\mathrm{fw}}^6\frac{1}{R^2}\int_0^R dr_i\,r_i\\&\times\int_0^{\pi}\frac{d\phi}{[\sqrt{(R+\sigma_{\mathrm{fw}})^2-r_i^2\sin^2\phi}-r_i\cos\phi]^3}.\end{aligned} \tag{18}$$

The double integral was calculated numerically.

$\Psi_p(R)$ characterizes the fluid–wall interactions. The wall effect $[\Psi_p(R)]$ will be more significant for smaller pores. One would expect that as $R\to\infty$, the wall effect will become insignificant, therefore $\Psi_p(R)$ should approach 0. Indeed, as shown in Fig. 1, $\Psi(R)$ approaches 0 as R gets larger.

C. Fluid–fluid potential

The attraction term of the interaction potential between one molecule in r_i and another fluid molecule in r_j a distance r_{ij} from the first one is given by

$$u_{\mathrm{ff}}^{\mathrm{disp}}(r_{ij})=-\frac{4\epsilon_{\mathrm{ff}}\sigma_f^6}{r_{ij}^6}\quad\text{for } r_{ij}>\sigma_f. \tag{19}$$

Then

$$\langle U_{\mathrm{ff}}^{\mathrm{disp}}\rangle_0=\tfrac{1}{2}\int_V dr_i\int_V dr_j\,\rho_0(r_i,r_j)u_{\mathrm{ff}}^{\mathrm{disp}}(r_{ij}), \tag{20}$$

where $\rho_0(r_i,r_j)$ is the pair distribution function, given by[10]

$$\rho_0(r_i,r_j)=\rho_0(r_i)\rho_0(r_j)g(r_i,r_j). \tag{21}$$

$g(r_i,r_j)$ is the pair correlation function, which in the mean-field approach is given as

$$g(r_i,r_j)=\begin{cases}0, & r_{ij}<\sigma_f\\ 1, & r_{ij}\geqslant\sigma_f.\end{cases} \tag{22}$$

Therefore,

$$\langle U_{\mathrm{ff}}^{\mathrm{disp}}\rangle_0=\frac{1}{2}\int_V dr_i\int_V dr_j\,\rho_p\rho_p g(r_i,r_j)\left(\frac{-4\epsilon_{\mathrm{ff}}\sigma_f^6}{r_{ij}^6}\right)$$

$$=-2\epsilon_{\mathrm{ff}}\sigma_f^6\rho_p^2\int_V dr_i\int_V dr_j\,g(r_i,r_j)r_{ij}^{-6}. \quad (23)$$

Transforming Eq. (23) from $\{r_i,r_j\}$ to $\{r_i,r_{ij}\}$, we get

$$\langle U_{\mathrm{ff}}^{\mathrm{disp}}\rangle_0=-2\epsilon_{\mathrm{ff}}\sigma_f^6\rho_p^2\int_0^H dh\int_0^{2\pi}d\theta\int_0^R dr_i\,r_i\int_{V(r_i)}dr_{ij}\,r_{ij}^{-6}$$

$$=-4\pi H\epsilon_{\mathrm{ff}}\sigma_f^6\rho_p^2\int_0^R dr_i\,r_i\int_{V(r_i)}dr_{ij}\,r_{ij}^{-6}. \quad (24)$$

Transforming Eq. (24) into cylindrical coordinates, where the second cylindrical coordinate system will have its center on the first molecule, one obtains

$$\langle U_{\mathrm{ff}}^{\mathrm{disp}}\rangle_0=-4\pi H\epsilon_{\mathrm{ff}}\sigma_f^6\rho_p^2\int_0^R dr_i\,r_i \times\left[\int_0^{2\pi}d\phi\int_{-\infty}^{+\infty}dz\int_{\rho_{\min}}^{\rho_{\max}}d\rho\,\rho(\rho^2+z^2)^{-3}\right]. \quad (25)$$

Using the symmetry on ϕ and z,

$$\langle U_{\mathrm{ff}}^{\mathrm{disp}}\rangle_0=-16\pi H\epsilon_{\mathrm{ff}}\sigma_f^6\rho_p^2\int_0^R dr_i\,r_i \times\left[\int_0^{\pi}d\phi\int_0^{\infty}dz\int_{\rho_{\min}}^{\rho_{\max}}d\rho\,\rho(\rho^2+z^2)^{-3}\right]. \quad (26)$$

Splitting the integration range for z from $|_0^\infty$ to $|_0^{\sigma_f}+|_{\sigma_f}^\infty$, the expression for $\langle U_{\mathrm{ff}}^{\mathrm{disp}}\rangle_0$ can be transformed to

$$\langle U_{\mathrm{ff}}^{\mathrm{disp}}\rangle_0=-16\pi H\epsilon_{\mathrm{ff}}\sigma_f^6\rho_p^2 I_{\mathrm{ff}}, \quad (27)$$

where

$$I_{\mathrm{ff}}=\int_0^R dr_i\,r_i\int_0^{\pi}d\phi\int_0^{\sigma_f}dz\int_{\sqrt{\sigma_f^2-z^2}}^{\rho_{\max}}d\rho\,\rho(\rho^2+z^2)^{-3} +\int_0^R dr_i\,r_i\int_0^{\pi}d\phi\int_{\sigma_f}^{\infty}dz\int_0^{\rho_{\max}}d\rho\,\rho(\rho^2+z^2)^{-3} \quad (28)$$

and the upper limit in ρ, $\rho_{\max}$, depends on z as well. Applying Eq. (A6) and Fig. 10 one finds the following:

For $z=0$ to σ_f,

$$\rho_{\max}=\begin{cases}[\sqrt{R^2-r_i^2\sin^2\phi}-r_i\cos\phi] \\ \quad \text{for } [\sqrt{R^2-r_i^2\sin^2\phi}-r_i\cos\phi]\geqslant\sqrt{\sigma_f^2-z^2} \\ \sqrt{\sigma_f^2-z^2} \\ \quad \text{for } [\sqrt{R^2-r_i^2\sin^2\phi}-r_i\cos\phi]<\sqrt{\sigma_f^2-z^2}.\end{cases} \quad (29)$$

For $z=\sigma_f$ to ∞,

$$\rho_{\max}=\sqrt{R^2-r_i^2\sin^2\phi}-r_i\cos\phi. \quad (30)$$

Thus,

$$\langle U_{\mathrm{ff}}^{\mathrm{disp}}\rangle_0=-a_p(R)N\rho_p, \quad (31)$$

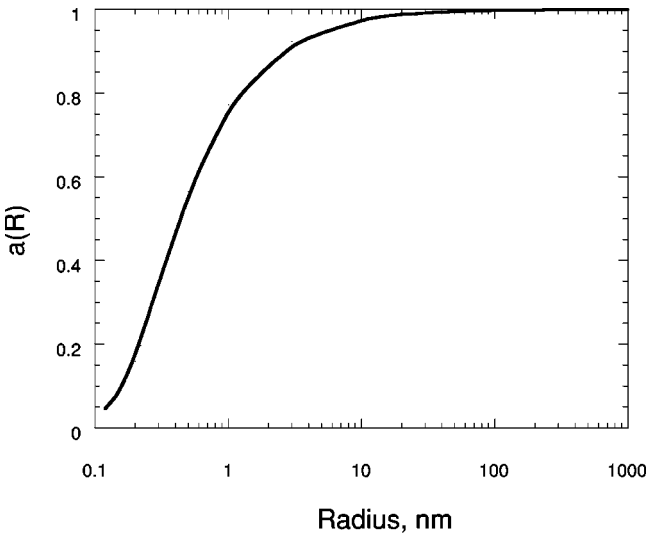

FIG. 2. The normalized fluid–fluid interactions potential. $a(R)=a_p(R)/a_b$ is calculated based on Eq. (35).

where

$$a_p(R)=\frac{16\epsilon_{\mathrm{ff}}\sigma_f^6}{R^2}I_{\mathrm{ff}}. \quad (32)$$

The fluid–fluid interaction parameter for the bulk fluid is given:

$$a_b=\frac{8\pi\sigma_f^3\epsilon_{\mathrm{ff}}}{3}. \quad (33)$$

From Eqs. (32) and (33) we can find:

$$a_p(R)=a(R)a_b, \quad (34)$$

where

$$a(R)=\frac{6\sigma_f^3}{\pi R^2}I_{\mathrm{ff}}. \quad (35)$$

In a confined fluid, the molecules close to the wall do not have the possibility to interact with as many fluid neighbors as a molecule in a bulk fluid. However, as the radius R becomes larger, the confined fluid becomes less distinguishable from the bulk fluid. In the limit, as $R\to\infty$, one should expect $a_p(R)\to a_b$, or, equivalently, $a(R)\to 1$. As shown in Fig. 2, $a(R)$ goes to 1 as R goes to infinity, as expected.

D. Hydrogen bond interactions

Truskett *et al.*[7,8] proposed a model for the hydrogen bonding of a water-like fluid. Recently, we analyzed their model in some detail and offered a few modifications.[9]

The strength of each hydrogen bond will depend on the distance between atoms participating in the bond as well as their relative angles. It is required here that two molecules be within a distance of from σ_f to r_0 from each other in order for them to form a hydrogen bond. The spherical region between σ_f and r_0 is termed the hydrogen bonding shell. In order to participate in the hydrogen bonding, two molecules must be close enough, but they should also have a favorable orientation. Jedlovszky *et al.*[11] studied the water structure by

molecular dynamics and reverse Monte Carlo simulations. They showed that the number of hydrogen bonds and their energy was dependent on the limiting angle between atoms participating in the hydrogen bonding. Truskett *et al.*[8] notes that the orientational dependence of hydrogen bond is crucial for reproducing density anomalies of water.

In this model we account in a very simplified way for the orientation dependence of hydrogen bonding. Specifically, it is assumed that, if there are four or fewer neighbor molecules in the hydrogen bonding shell, they will be oriented in a such way that all of them participate in hydrogen bonding. But, if there are more than four molecules in the hydrogen bonding shell, then the orientation becomes unfavorable for all four potential hydrogen bonds to be formed. For simplicity, we assume that for every molecule in the hydrogen bonding shell in excess of four, one hydrogen bond is broken. It follows that if there are eight or more molecules in the hydrogen bonding shell of a molecule, that the molecules are not able to form hydrogen bonds at all. This condition will account for the open structure of water without the need of the cavity restriction, introduced by Truskett *et al.*[8] Note that the model presented here ignores the temperature dependence of the hydrogen bonding. However, our focus at this time is on the behavior of water confined in pores at ambient conditions. Thus, we are not examining phase transitions of water and densities anomalies. As explained previously,[9] the original model presented by Truskett *et al.*[7] for water confined in slit pores was incapable of describing bulk and confined water properties at ambient conditions. Therefore, ignoring the temperature dependence of hydrogen bonding is not considered crucial in our context.

If p_j defines the probability that j molecules are in the hydrogen bonding shell, and ϵ^{HB} is the energy of one hydrogen bond, then the energy of hydrogen bonds of a given molecule in the bulk fluid will be given by

$$U_{(\mathrm{HB})}=\tfrac{1}{2}C\left[\sum_{j=1}^{4} jp_j\epsilon^{\mathrm{HB}}+\sum_{5}^{7}(8-j)p_j\epsilon^{\mathrm{HB}}\right], \tag{36}$$

where the sum is divided by two since the hydrogen bonding energy is a pairwise contribution. The constant C accounts for uncertainties on the ϵ^{HB} values and on the orientational dependence of the hydrogen bond. It also accounts for the fact that some hydrogen bonds might be ''broken,''[12] i.e., not all the molecules that fulfill geometrical criteria participate in hydrogen bonding. Its value is determined in Sec. IV, based on the properties of coexisting liquid and vapor phase at ambient conditions.

For the bulk fluid, Torquato[13] derived the expression for the probability that there are j molecules in the hydrogen bonding shell as

$$p_j^b=\frac{1}{j!}\left(\frac{24\eta_b}{\sigma_f^3}\int_{\sigma_f}^{r_0}dr\,r^2G(r)\right)^j \times\exp\left(-\frac{24\eta_b}{\sigma_f^3}\int_{\sigma_f}^{r_0}dr\,r^2G(r)\right), \tag{37}$$

where

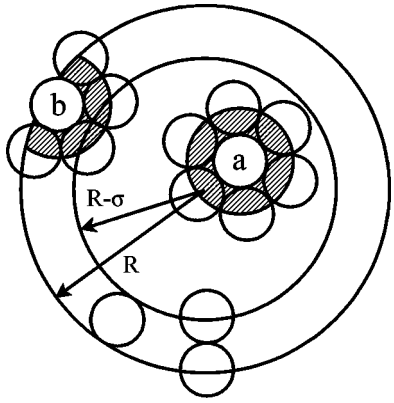

FIG. 3. Schematic presentation of a molecule a in the middle section ($0<r<R-\sigma_f$), and of a molecule b in the outside layer ($R-\sigma_f<r<R$) of the confined fluid.

$$G(r)=\begin{cases}0, & r\leqslant\sigma_f\\ a_0+\dfrac{a_1}{(r/\sigma_f)}+\dfrac{a_2}{(r/\sigma_f)^2}, & r\geqslant\sigma_f\end{cases} \tag{38}$$

and

$$\begin{aligned}a_0&=1+4\eta_pG(\sigma_f),\\ a_1&=\frac{3\eta_p-4}{2(1-\eta_p)}+2(1-3\eta_p)G(\sigma_f),\\ a_2&=\frac{2-\eta_p}{2(1-\eta_p)}+(2\eta_p-1)G(\sigma_f),\\ G(\sigma_f)&=\frac{1-\eta_p/2}{(1-\eta_p)^3}.\end{aligned} \tag{39}$$

η_b is the packing fraction, which for bulk fluid is defined as

$$\eta_b=\frac{\pi\sigma_f^3}{6}\rho_b. \tag{40}$$

Equation (36) is suggested for the bulk fluid, where the water molecules can form up to four hydrogen bonds. However, one can expect that molecules close to the pore wall have a different hydrogen bonding capability than a molecule in bulk. Rovere *et al.*[14] performed a molecular dynamic simulation of water confined in a cylindrical (Vycor glass) pore with diameter 4 nm. Their analysis revealed that purely geometrical confinement is responsible for the reduction of the number of hydrogen bonds at the fluid–wall interface. For molecules as far from the wall as 0.8 nm, the hydrogen bonding capabilities were the same as for bulk fluid. For simplicity, the confined fluid is divided into two layers. For the middle section of the porous fluid, $0<r<R-\sigma_f$ (see Fig. 3), the scenario is similar to the bulk fluid described previously. Therefore, the energy of the hydrogen bond would be given by Eq. (36); however, the probability p_j^p of finding j molecules in the hydrogen bonding shell of a molecule in the middle section of the pores is given by Eq. (37), where

$$\eta_p=\frac{\pi\sigma_f^3}{6}\rho_p \tag{41}$$

is used instead of η_b.

However, for a water molecule too close to the wall, $R-\sigma_f<r<R$ (see Fig. 3), it is impossible to participate in four hydrogen bonds. Therefore, the hydrogen bonding capabilities of a molecule in the bulk fluid are different from that of a confined molecule. The maximum number of hydrogen bonds that a molecule in the outside layer can form is proportional to the volume of spheres with radius σ_f enclosed within the cylinder with radius R (the shaded area in Fig. 3). Using the results from the Appendix B, this volume (per unit volume of outside layer) is given by

$$V_0=\frac{8\rho_p}{R^2-(R-\sigma_f)^2}I_{\mathrm{HB}}, \tag{42}$$

where I_{HB} is

$$I_{\mathrm{HB}}=\int_{R-\sigma_f}^{R}d\rho\rho\int_{\rho-\sigma_f}^{R}dr\,r \times\int_0^{\sqrt{\sigma_f^2-(\rho-r)^2}}dz\cos^{-1}\left(\frac{r^2-\sigma_f^2+z^2+\rho^2}{2r\rho}\right). \tag{43}$$

The ratio of the packing fractions of the outside layer with the middle section would be

$$\frac{\eta_p(\mathrm{outside})}{\eta_p(\mathrm{middle})}=\frac{8\rho_p}{R^2-(R-\sigma_f)^2}I_{\mathrm{HB}}\frac{3}{4\pi\sigma_f^3\rho_p} =\frac{6I_{\mathrm{HB}}}{\pi\sigma_f^3[R^2-(R-\sigma_f)^2]}. \tag{44}$$

It is assumed that the hydrogen bonding energy for the outside layer is equal to the energy of the middle section multiplied by the ratio of the packing fractions of the outside and middle sections. Then the coefficient in front of the hydrogen bonding term for the aggregate confined fluid will be

$$H(R)=\frac{1}{\pi R^2}\left[\pi(R-\sigma_f)^2+\pi[R^2-(R-\sigma_f)^2]\times\frac{6I_{\mathrm{HB}}}{\pi\sigma_f^3[R^2-(R-\sigma_f)^2]}\right] =\left(1-\frac{\sigma_f}{R}\right)^2+\frac{6I_{\mathrm{HB}}}{\pi R^2\sigma_f^3}. \tag{45}$$

Therefore, the hydrogen bonding energy for the fluid confined in the pores will be

$$U_{\mathrm{HB}}^p=H(R)\frac{C}{2}\left[\sum_{j=1}^{4}jp_j^p\epsilon^{\mathrm{HB}}+\sum_{5}^{7}(8-j)p_j^p\epsilon^{\mathrm{HB}}\right]. \tag{46}$$

E. Equation of state

From Eqs. (1), (12), (17), (31), and (46) we obtain the expression for the Helmholtz free energy:

$$F=-N\beta^{-1}\left(\ln\left(\frac{1-\rho_p b_p(R)}{\rho_p\Lambda^3}\right)+1\right)-Na_p(R)\rho_p+N\Psi_p(R) +H(R)\frac{NC\epsilon^{\mathrm{HB}}}{2}\left(\sum_{j=1}^{4}jp_j^p+\sum_{5}^{7}(8-j)p_j^p\right). \tag{47}$$

The pressure of the confined fluid can be defined as [see Eq. (2)]

$$P_{\parallel}=-\frac{1}{\pi R^2}\left(\frac{\partial F}{\partial H}\right)_{N,T}=\rho_p^2\left(\frac{\partial(F/N)}{\partial\rho_p}\right)_{N,T}. \tag{48}$$

Finally, referring to Eq. (47), the mean-field equation of state gives the confined fluid pressure as

$$P_{\parallel}=\frac{\rho_p}{\beta(1-\rho_p b_p(R))}-a_p(R)\rho_p^2 +\rho_p^2H(R)\frac{C\epsilon^{\mathrm{HB}}}{2}\left(\sum_{j=1}^{4}j\frac{\partial p_j^p}{\partial\rho_p}+\sum_{j=5}^{7}(8-j)\frac{\partial p_j^p}{\partial\rho_p}\right). \tag{49}$$

In the limit, for $R\to\infty$, $P_{\parallel}$ goes to the bulk fluid pressure, P_b:

$$P_b=\frac{\rho_b}{\beta(1-\rho_b b_b)}-a_b\rho_b^2+\rho_b^2\frac{C\epsilon^{\mathrm{HB}}}{2} \times\left(\sum_{j=1}^{4}j\frac{\partial p_j^b}{\partial\rho_b}+\sum_{j=5}^{7}(8-j)\frac{\partial p_j^b}{\partial\rho_b}\right). \tag{50}$$

IV. PARAMETERS

The model presented here is very sensitive to the choice of parameters. It was first attempted to apply the parameters suggested by Truskett *et al.*[7,8] However, as explained in Giaya and Thompson,[9] some of the parameter values used in Truskett *et al.*,[7,8] while giving a reasonable global description of water's phase behavior, may not be appropriate for water at 298 K and 1 bar.[9] The parameters used in this study were determined based on the properties of bulk water at ambient conditions. Truskett *et al.*[7,8] used a value of $1.04\sigma_f$ for the hydrogen bonding shell, where σ_f was taken to be 3.11 Å. Care has to be taken in choosing the r_0. Specifically, we looked at the term

$$f(r_0)=\left(\sum_{j=1}^{4}j\frac{\partial p_j^b}{\partial\rho_b}+\sum_{j=5}^{7}(8-j)\frac{\partial p_j^b}{\partial\rho_b}\right), \tag{51}$$

which appears in Eq. (50). Hydrogen bonding provides a cohesive contribution to the liquid water under normal conditions. Therefore, the above-given term $[f(r_0)]$ must be positive. In Fig. 4 the value of the above-given term is plotted against the value r_0. For $r_0=1.04\sigma_f$, the model predicts the hydrogen bonding contribution to not be cohesive. Therefore, a value of $r_0=1.039\sigma_f$ was used instead.

The value of b_b was determined through Eq. (9) to be 1.4815×10^{-5} m^3/mol. The energy of a hydogen bond ϵ^{HB} was taken 20 kJ/mol.[15] Then, as suggested in Giaya and Thompson,[9] the parameters a_b and C were chosen to satisfy

$$P|_{\rho=0.997\,04\ \mathrm{g/cm^3}}=1.01\times10^5\ \mathrm{Pa},\quad P|_{\rho=23.05\times10^{-6}\ \mathrm{g/cm^3}}=3167\ \mathrm{Pa},\quad \mu|_{\rho=0.997\,04\ \mathrm{g/cm^3}}=\mu|_{\rho=23.05\times10^{-6}\ \mathrm{g/cm^3}}. \tag{52}$$

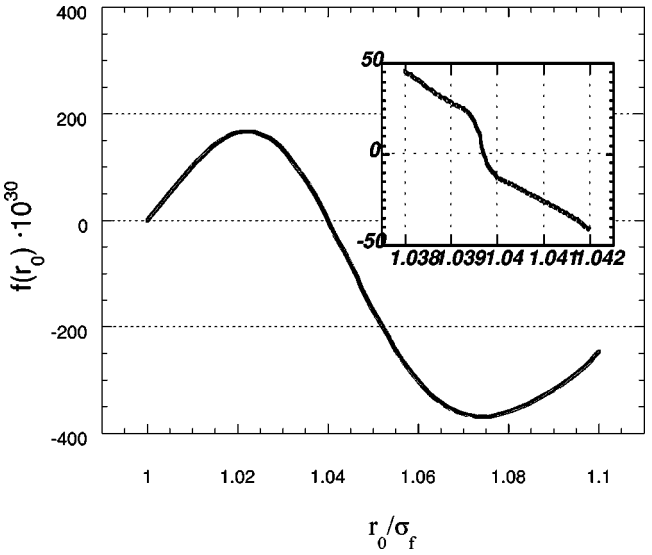

FIG. 4. Determining the hydrogen bonding shell parameter, r_0. $f(r_0)$ is defined by Eq. (51).

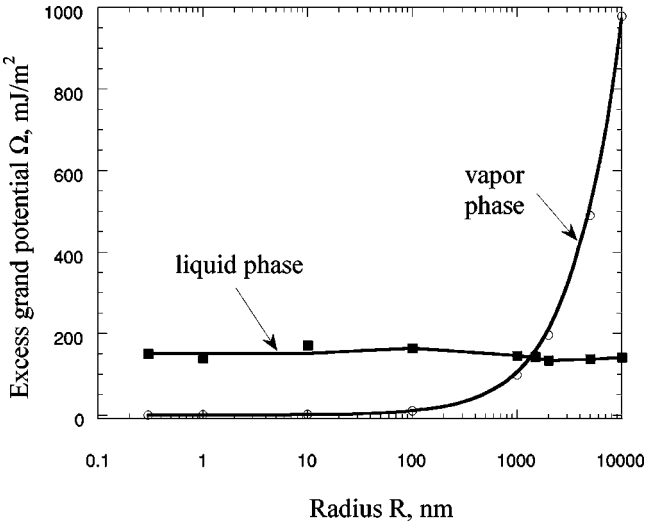

FIG. 5. Excess grand potential $(P_{\parallel}-P^{\text{bulk}})R$ for liquid and vapor phases of the confined fluid. Bulk fluid is liquid ($\rho_b=0.997\,04$ g/cm^3) at 298 K. It is assumed that there are no interactions between the fluid and wall ($\epsilon_{\text{fw}}=0$).

The first condition requires that water have a liquid density of 0.997 04 g/cm^3 at 298 K and 1.01×10^5 Pa.[16] The second condition requires that water have a saturated vapor density of 23.05×10^{-6} g/cm^3 at 298 K and attains the partial pressure of saturated water vapor of 3.167 kPa.[16] The third condition requires the coexistence of the water liquid and vapor phases at ambient conditions. Solving these equations simultaneously gave $a_b=0.090\,63$ Pam^6 mol^{-2} and $C=0.937\,087$.

V. RESULTS AND DISCUSSIONS

The model derived here was used to predict the density of the stable phase of the fluid inside the pores, knowing the density of the fluid outside the pores. At equilibrium, the chemical potential of fluid inside the pore must be equal to the chemical potential of bulk fluid outside the pores. Therefore, the difference $\mu_p-\mu_b$ must be equal to zero. Thus, at equilibrium [using Eqs. (C2) and (C3)]

$$\Delta\mu\equiv 0=\mu_p-\mu_b=\beta^{-1}\ln\frac{\rho_p}{\rho_b}\frac{1-\rho_b b_b}{1-\rho_p b_p(R)}+\beta^{-1}\frac{\rho_p b_p(R)}{1-\rho_p b_p(R)}-\beta^{-1}\frac{\rho_b b_b}{1-\rho_b b_b}-2(a_p(R)\rho_p-a_b\rho_b)+\Psi_p(R)$$
$$+H(R)\frac{C\epsilon^{\text{HB}}}{2}\left\{\left(\sum_{j=1}^{4} jp_j^p+\sum_{j=5}^{7}(8-j)p_j^p\right)+\rho_p\left(\sum_{j=1}^{4} j\frac{\partial p_j^p}{\partial\rho_p}+\sum_{j=5}^{7}(8-j)\frac{\partial p_j^p}{\partial\rho_p}\right)\right\}$$
$$-\frac{C\epsilon^{\text{HB}}}{2}\left\{\left(\sum_{j=1}^{4} jp_j^b+\sum_{j=5}^{7}(8-j)p_j^b\right)-\rho_b\left(\sum_{j=1}^{4} j\frac{\partial p_j^b}{\partial\rho_b}+\sum_{j=5}^{7}(8-j)\frac{\partial p_j^b}{\partial\rho_b}\right)\right\}. \quad (53)$$

In adsorption equilibrium experiments, ρ_b, T, and R are fixed and known. Therefore, $\Delta\mu$ depends only on ρ_p.

The first case considered was of a hard wall pore (i.e., with $\epsilon_{\text{fw}}=0$). The bulk fluid outside the pores was assumed to be liquid water of density 0.997 04 g/cm^3 at temperature of 298 K and pressure of 1 atm. Densities of the vapor and liquid phases of the confined water were calculated using Eq. (53). Of three solutions for ρ_p, the value of ρ_p that minimizes the grand potential Ω (or maximizes pressure $P_{\parallel}$—Refs. 6 and 7), must be selected. The excess potentials, $(P_{\parallel}-P^{\text{bulk}})R$, of the confined vapor and liquid phases as functions of the pore radius are plotted in Fig. 5. As shown in Fig. 5, for pore radii smaller than 1500 nm, the vapor phase is stable inside the pores; for pores bigger than it $\sim$1,500 nm, liquid is the stable phase. In other words, for a hard wall pore with $\epsilon_{\text{fw}}=0$, a liquid at ambient conditions ($T=298$ K and $P=1$ atm) will exist inside the pores only if its radius is bigger than 1500 nm.

This critical radius seems surprisingly large, especially if one notes from Figs. 1 and 2 that the effects of confinement on fluid–fluid and fluid–wall interactions vanish rapidly with the pore radius. Indeed, at 1500 nm radius, for example, the normalized fluid–fluid van der Waals interactions $(a_p(R)/a_b)$, excluded volume parameter $(b_p(R)/b_b)$, and hydrogen bonding interactions parameter $[H(R)]$ are, respectively, 0.999 947, 0.999 961, and 0.999 922. These very small

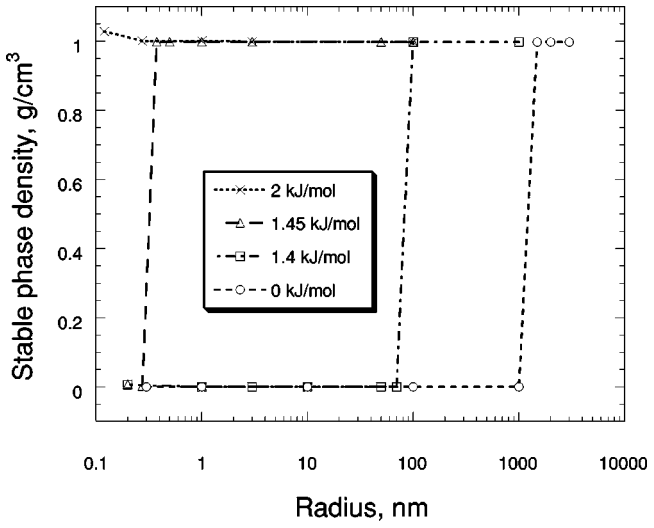

FIG. 6. Density of the stable phase of the confined fluid vs the pore radius for four arbitrary values of the fluid–wall interaction potential. Bulk fluid is liquid ($\rho_b = 0.997\,04$ g/cm^3) at 298 K.

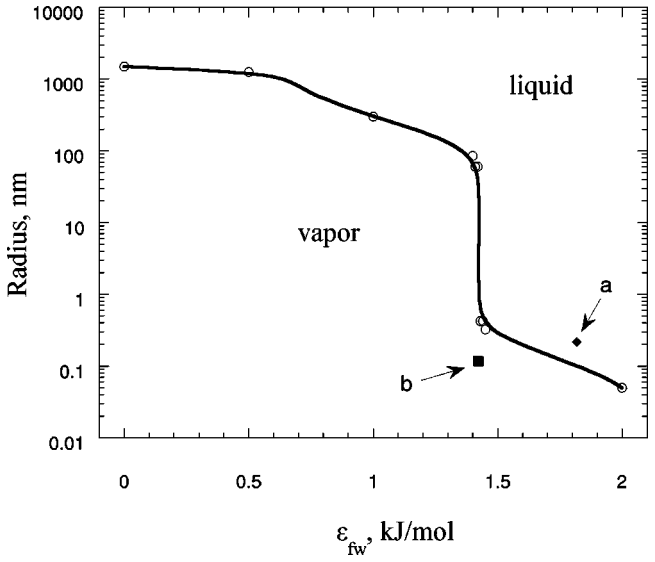

FIG. 7. Liquid–vapor coexistence curve for the confined fluid in the ϵ_{fw}–R plane while bulk fluid is liquid ($\rho_b = 0.997\,04$ g/cm^3) at 298 K. Points a and b represent DAY and silicalite samples (Ref. 1).

deviations of confined fluid parameters from the bulk fluid parameters cause the density of the liquid branch to be very close to, but smaller than, the bulk liquid density (e.g., 0.997 039 7 versus 0.997 04 g/cm^3). However, under these circumstances, the very small decrease of the density causes the pressure value to be lower than the pressure of the vapor phase, hence the liquid phase becomes thermodynamically unstable. In effect, this seemingly insignificant reduction in the predicted liquid density, stemming from the disruption of the fluid molecules within ~10 nm from the wall, is sufficient to lower the predicted pressure by a significant amount. While it is hard to imagine that vapor will be the stable phase for radii up to 1500 nm, it is worth noting that the case under consideration is for the hard wall, which has no interactions at all with the confined fluid. In reality, even the most hydrophobic wall would interact with confined fluid via van der Waals forces. The transition point shown in Fig. 5 is in agreement with the results reported by Lum *et al.*,[17] who showed that, even for relatively large distances between two hard parallel plates, the confined liquid water was thermodynamically less stable than its vapor. They also predicted this transition to occur at a width of ~1500 nm for slit pores. It was expected that this transition would occur at a larger cylindrical pore dimension due to the two-dimensional confinement compared to one dimension for parallel plates.

In Fig. 6 the density of the stable phase is plotted against pore radius for values of fluid–wall potential, respectively, of 0, 1.4, 1.45, and 2 kJ/mol. Again, in this case the bulk fluid was assumed to be liquid at 298 K and 1 atm. The density of the wall was assumed to be 1.827×10^5 (mole atoms)/m^3. As shown in Fig. 6, the radius at which the transition from vapor to liquid occurs depends on the fluid–wall potential. As the fluid–wall interaction increases, the pore radius for which the transition occurs decreases. For high enough values of the fluid–wall potential ($\epsilon_{fw} > 2$ kJ/mol) the stable phase inside the pores is liquid water for any value of R. The impact of a strong attractive force is to promote condensation of a liquid phase.

From Fig. 5 we saw that the radius for which vapor and liquid phase could coexist is 1500 nm for hard wall pores. Similarly, the radius of phase coexistence for pores with varying values of ϵ_{fw} was determined and the results are plotted in Fig. 7. An interesting feature of Fig. 7 is that the radius corresponding to phase coexistence is very sensitive to the value of the fluid–wall potential in some regions. Seemingly minor variations on evaluating ϵ_{fw} values from different adsorption data points could lead to uncertainty on determining the stable phase of the confined fluid.

If ρ_p and ρ_b of a given sample are known from experimental vapor phase adsorption data, then one can solve Eq. (53) for ϵ_{fw}. Hence, from Eqs. (53) and (17) we can get

$$\epsilon_{fw} = \left\{ \left(2(a_p(R)\rho_p - a_b\rho_b) - \beta^{-1} \ln \frac{\rho_p(1-\rho_b b_b)}{\rho_b(1-\rho_p b_p(R))} - \beta^{-1} \frac{\rho_p b_p(R)}{1-\rho_p b_p(R)} + \beta^{-1} \frac{\rho_b b_b}{1-\rho_b b_b} \right.\right.$$
$$- H(R) \frac{C\epsilon^{HB}}{2} \left\{ \left(\sum_{j=1}^{4} j p_j^p + \sum_{j=5}^{7} (8-j) p_j^p \right) + \rho_p \left(\sum_{j=1}^{4} j \frac{\partial p_j^p}{\partial \rho_p} + \sum_{j=5}^{7} (8-j) \frac{\partial p_j^p}{\partial \rho_p} \right) \right\}$$
$$\left.\left. + \frac{C\epsilon^{HB}}{2} \left\{ \left(\sum_{j=1}^{4} j p_j^b + \sum_{j=5}^{7} (8-j) p_j^b \right) - \rho_b \left(\sum_{j=1}^{4} j \frac{\partial p_j^b}{\partial \rho_b} + \sum_{j=5}^{7} (8-j) \frac{\partial p_j^b}{\partial \rho_b} \right) \right\} \right\} \frac{1}{\Psi(R)}. \quad (54)$$

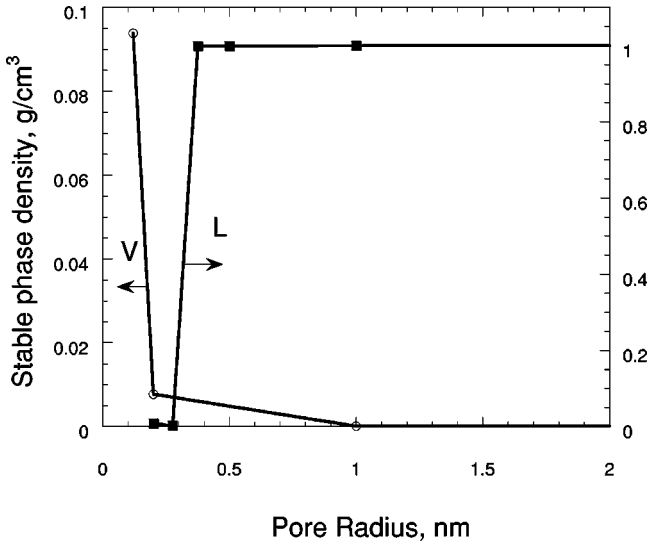

FIG. 8. Density of the stable phase of the confined fluid vs pore radius for two cases: L—bulk fluid is liquid ($\rho_b = 0.997\,04$), and V—bulk fluid is vapor ($\rho_b = 20.93 \times 10^{-6}$ g/cm^3) at temperature 298 K.

In this study, ϵ_{fw} values for DAY and silicalite samples were determined based on the water TGA measurements[1] and Eq. (54). Their values were 1.818 and 1.422 kJ/mol, respectively. a and b in Fig. 7 represent those samples. It is interesting to see that, based on Fig. 7, in the presence of bulk liquid at ambient conditions, the stable phase inside the silicalite pores is predicted to be a vapor phase. Under the same conditions, the stable phase inside the pores of the DAY sample is predicted to be liquid. These predictions show that very small changes in the pore radius and fluid–wall potential can cause significant changes in the state of the confined fluid. Consider a hypothetical zeolitic material with fluid–wall parameter $\epsilon_{fw} = 1.45$ kJ/mol. From a practical point of view, it is interesting to know how the density of the stable phase inside the pores would change as the pore radius varies. The density of the stable fluid phase in the pores is plotted in Fig. 8 for two cases of bulk fluid: liquid of density 0.99704 g/cm^3 (L), and vapor of density 20.93 $\times 10^-6$ g/cm^3 (V). In the case of a bulk vapor phase, the fluid in the smaller pores will feel stronger wall attraction due to the small pore size, therefore the density of the stable phase is relatively high, but still vapor. As the radius is increased, the density of the pore fluid is decreased. Therefore, for gas phase applications, the material with larger pores would be more hydrophobic. In the second case, when there is liquid water outside the pores, the scenario is reversed. A liquid phase is unstable in smaller pores, but becomes stable for larger pores. Therefore, for liquid phase applications, the material with smaller pores will be more hydrophobic.

There are some cases where it is beneficial to rank different materials based on their hydrophobicity. Intuitively, the more hydrophobic material should have a lower water concentration inside the pores. Several definitions have been offered for a "hydrophobicity index" (Anderson and Klinowski,[18] Weitkamp *et al.*,[19] Olson *et al.*,[20] Giaya *et al.*[1]). Based on these definitions and the water adsorption/desorption data, DAY and silicalite samples were recently analyzed.[1] Gas phase water adsorption/desorption data showed that the DAY sample was as hydrophobic as the silicalite sample, if not more so. However, CVOC adsorption out of dilute water solutions showed that the silicalite was more organophilic, presumably due to its repulsion of water molecules. As shown previously, none of the above-mentioned hydrophobicity indices could explain the relative behavior of silicalite and DAY samples in both vapor and liquid systems.

The hydrophobicity of zeolitic materials is based on many factors (Si/Al ratio, structural defects, cations present in the structure, synthesis and postsynthesis treatments, etc.). silicalite is synthesized as an all silica ZSM-5, and, since it contains essentially no Al, it is believed to be very hydrophobic.[21] DAY, on the other hand, is a dealuminated Y sample, and its hydrophobicity will certainly depend on the dealumination technique. At best, the pore wall surface of DAY can be as hydrophobic as the pore wall surface of as-synthesized silicalite. So the ϵ_{fw} for DAY/water should be equal to (for the most hydrophobic DAY) or larger than the ϵ_{fw} value for silicalite/water. Applying the model presented here to the water TGA data given in Giaya *et al.*[1] it was found that the fluid wall potential of DAY was indeed higher than that of silicalite sample (1.818 versus 1.422 kJ/mol). So, based on the ϵ_{fw} values, one can conclude that the silicalite sample was more hydrophobic than the DAY sample used in the study. However, the vapor phase adsorption/desorption data presented earlier[1] showed that water adsorption on silicalite was slightly higher than water adsorption on DAY. The model derived here predicts those results, i.e., the density of the stable phase inside the silicalite pores is higher than the density of the stable phase inside the DAY pores when exposed to water vapor. This is explained by noting that the wall effect is more significant due to the smaller pores of silicalite. The situation is reversed when liquid water is present outside the pores. In this case, as shown previously, the very small confinement space in silicalite disrupts the dispersive interactions and hydrogen bonds to the extent that liquid water cannot exist inside the pores. However, the cages of DAY are big enough to accommodate the liquid phase inside it under those conditions. That causes the silicalite to appear more hydrophobic than DAY when liquid water is concerned.

From the above-presented discussion, one can see that it is not easy to have a single definition of the hydrophobicity index with universal applicability. The hydrophobicity depends on the adsorbent chemical composition and structure of the surface (hence ϵ_{fw}) as well as the pore size. Additionally, the relative hydrophobicity of different microporous materials will depend on whether there is liquid or vapor water outside the pores.

VI. CONCLUSIONS

Water-like fluid confined in cylindrical pores has been studied applying the perturbation theory. It was assumed that the fluid inside the pores was homogenous. The fluid–fluid hydrogen bonding interactions were treated based on the model presented by Truskett *et al.*[8] as modified by Giaya and Thompson.[9] The model simplifies the dependence of hydro-

gen bonding on the relative orientation. The fluid–wall hydrogen bonding interactions were not considered. The model was used to predict the dependence of the density of the water inside the pores on the density outside the pores, the pore radius, and the affinity of the wall for water molecules. Although a simple model, its predictions seems to agree well with experimental results.

The analysis allows one to predict the stable fluid phase in the pores at equilibrium with the fluid outside the pores. With saturated liquid water outside the pores, the fluid inside the pores is a vapor until the pore radius is increased to a critical size, after which it is a liquid. The critical pore radius is rather large, ~ 1500 nm, for hard wall pores, for which $\epsilon_{fw}=0$, and decreases to essentially zero rather dramatically as ϵ_{fw} is increased to about 2 kJ/mol. The locus of points separating stable vapor and liquid phases in the pores with liquid water outside the pores showed quite clearly that as the value of ϵ_{fw} increased, the critical radius decreased precipitously.

The analysis also showed that quite the opposite was predicted when saturated vapor was outside the pores. That is, for hypothetical materials having the same ϵ_{fw} value as that computed for silicalite, the stable adsorbed fluid density decreased as the pore radius increased due to the decreased influence of the wall interactions. That is, as the pore radius increased, the region of interaction decreased relative to the volume of water molecules present. This result also stems from the fact that even silicalite has a nonzero fluid–wall interaction parameter, so there is some attractive interaction between fluid and wall molecules that causes the slight increase in vapor-like density in those pores.

Both the external liquid phase and the external vapor phase circumstances result in the stable adsorbed phase approaching the external fluid density once the pore radius becomes sufficiently large, as expected.

Finally, we note that the concept of a ''hydrophobicity'' of a material depends on the Si/Al ratio, structural defects, cations in the pores, and the inherent pore dimensions. However, it also was noted that the apparent behavior as a ''hydrophobic'' material depends on whether the water outside the pores is in the liquid or vapor state.

ACKNOWLEDGMENTS

The authors gratefully acknowledge the support of the National Science Foundation through Grant No. DGE-9355019. Additional support from Zodiac Pool Care, Inc., a Zodiac Company, of Smithfield, RI is gratefully acknowledged.

APPENDIX A: FLUID–WALL INTERACTION POTENTIAL

The interaction potential between a fluid molecule and an infinitesimal volume of a pore wall at a distance r from it is given by

$$u(r)=-4\epsilon_{fw}\left(\frac{\sigma_{fw}}{r}\right)^6. \tag{A1}$$

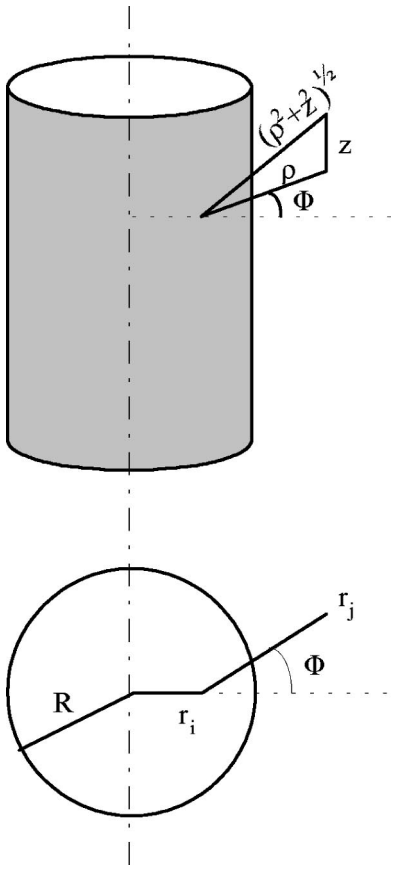

FIG. 9. Schematic side and top view of the cylindrical pore, used to determine the interaction of a fluid molecule at r_i with a wall molecule at r_j.

Then, the attraction potential of this fluid molecule at r_i with the pore wall is

$$U(r_i)=\rho_s\int_{\text{solid}} dr_j\, u(r_{ij}). \tag{A2}$$

Using cylindrical coordinates, and after some transformations (see Fig. 9), we get

$$U(r_i)=-16\rho_s\epsilon_{fw}\sigma_{fw}^6\int_0^{\pi} d\phi\int_{\rho_{\min}}^{\infty} d\rho_j\rho_j \times\left[\int_0^{\infty}\frac{dz_{ij}}{(z_{ij}^2+\rho_j^2)^3}\right]. \tag{A3}$$

Evaluating first the integral with respect to z_{ij}, then with respect to ρ_j, expression (A3) becomes

$$U(r_i)=-\pi\rho_s\epsilon_{fw}\sigma_{fw}^6\int_0^{\pi}\frac{d\phi}{\rho_{\min}^3}. \tag{A4}$$

Using the cosine theorem and Fig. 10 one finds

$$R^2=r_i^2+\rho_{\min}^2+2r_i\rho_{\min}\cos\phi. \tag{A5}$$

The positive root of Eq. (A5) with respect to $\rho_{\min}$ is

$$\rho_{\min}=\sqrt{R^2-r_1^2\sin^2\phi}-r_i\cos\phi. \tag{A6}$$

Substituting Eq. (A6) into Eq. (A4) gives

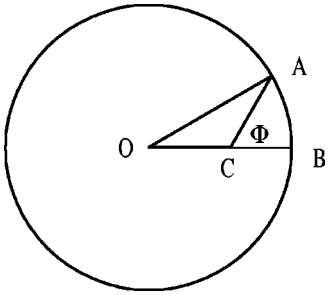

FIG. 10. Schematic presentation of a fluid molecule in the pore. $OA=R$, $OC=r_i$, $CA=\rho_{\min}$.

$$U(r_i) = -\pi\rho_s\epsilon_{\mathrm{fw}}\sigma_{\mathrm{fw}}^6 \times \int_0^{\pi} \frac{d\phi}{[\sqrt{(R+\sigma_{\mathrm{fw}})^2 - r_i^2\sin^2\phi} - r_i\cos\phi]^3}, \tag{A7}$$

where the expression under the integral is calculated numerically.

APPENDIX B: PACKING IN THE OUTSIDE SECTION OF THE CYLINDRICAL PORE

Let us consider spheres with radius σ_f centered in the cylindrical shell with $R-\sigma_f<r<R$ and height H. The objective of this section is to find the volume of these spheres enclosed in the cylinder with radius R. We limit this treatment to homogenous fluids, therefore

$$\rho_p = \frac{N}{\pi R^2 H}. \tag{B1}$$

Define $A^{\mathrm{int}}(r,\rho)$ as the projection on the surface of the cylinder with radius r of each of the spheres that have a distance ρ from the cylinder axis, where $r-\sigma_f/2\leqslant\rho\leqslant r+\sigma_f/2$:

$$A^{\mathrm{int}}(r,\rho) = \int\int r\,d\phi\,dz = 4r\int_0^{z_{\max}} dz \int_0^{\phi_{\max}(z)} d\phi \tag{B2}$$

or, after defining the limits in Eq. (B2) and integrating with respect to ϕ (see Fig. 11) we get

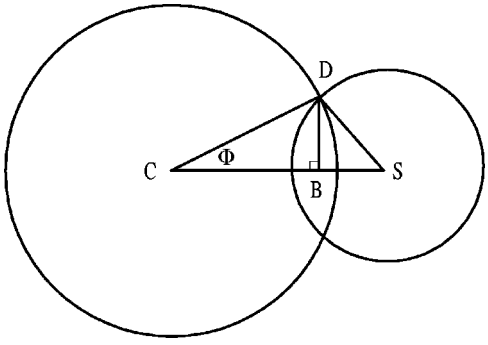

FIG. 11. Schematic illustrating the packing fraction for fluid in cylindrical pore. $DS=\sigma$, $\sigma=\sqrt{\sigma_f^2-z^2}$, $DC=r$, $CS=\rho$.

$$A^{x\mathrm{int}}(r,\rho) = 4r\int_0^{\sqrt{\sigma_f^2-(\rho-r)^2}} dz \times \cos^{-1}\left(\frac{r^2-\sigma_f^2+z^2+\rho^2}{2r\rho}\right). \tag{B3}$$

The volume of the spheres in the outside layer is

$$V = \int_{R-\sigma_f}^{R} d\rho\, 2\pi\rho\rho_p A^{\mathrm{int}}(r,\rho) = 8\pi\rho_p\int_{R-\sigma_f}^{R} d\rho\rho\int_{\rho-\sigma_f}^{R} dr\, r\int_0^{\sqrt{\sigma_f^2-(\rho-r)^2}} dz \times \cos^{-1}\left(\frac{r^2-\sigma_f^2+z^2+\rho^2}{2r\rho}\right). \tag{B4}$$

Dividing the above volume with the volume of the outside layer, gives the packing fraction in that layer:

$$V_0 = \frac{8\rho_p}{[R^2-(R-\sigma_f)^2]}\int_{R-\sigma_f}^{R} d\rho\,\rho\int_{\rho-\sigma_f}^{R} dr\, r \times \int_0^{\sqrt{\sigma_f^2-(\rho-r)^2}} dz\cos^{-1}\left(\frac{r^2-\sigma_f^2+z^2+\rho^2}{2r\rho}\right). \tag{B5}$$

Similarly, one can easily find that the packing fraction of the cylinder accessible to the sphere centers is

$$\eta_p(R) = \frac{8}{R^2}\rho_p\int_0^{R} dr\, r\int_{\rho_{\min}}^{\rho_{\max}} d\rho\,\rho\int_0^{\sqrt{(\sigma_f/2)^2-(\rho-r)^2}} dz \times \cos^{-1}\left(\frac{r^2-(\sigma_f/2)^2+z^2+\rho^2}{2r\rho}\right), \tag{B6}$$

where ρ_p is the fluid density, and

$$\rho_{\min} = \begin{cases} r-\sigma_f/2 & \text{if } r-\sigma_f/2>0 \\ 0 & \text{otherwise} \end{cases} \tag{B7}$$

and

$$\rho_{\max} = \begin{cases} r+\sigma_f/2 & \text{if } r+\sigma_f/2<R \\ R & \text{otherwise.} \end{cases} \tag{B8}$$

APPENDIX C: THE CHEMICAL POTENTIAL

The chemical potential for fluid inside the pores, μ_p, can be evaluated as follows:

$$\mu_p = \left(\frac{\partial F}{\partial N}\right)_{T,H}. \tag{C1}$$

Next, we take the derivative of F with respect to N term by term in Eq. (47) to get

$$\mu_p=\beta^{-1}\ln\frac{\rho_p\Lambda^3}{1-\rho_p b_p(R)}+\beta^{-1}\frac{\rho_p b_p(R)}{1-\rho_p b_p(R)}-2a_p(R)\rho_p+\Psi_p(R)+H(R)\frac{C\epsilon^{\mathrm{HB}}}{2}\times\left\{\left(\sum_{j=1}^{4} jp_j^p+\sum_{j=5}^{7}(8-j)p_j^p\right)+\rho_p\left(\sum_{j=1}^{4} j\frac{\partial p_j^p}{\partial\rho_p}+\sum_{j=5}^{7}(8-j)\frac{\partial p_j^p}{\partial\rho_p}\right)\right\}. \quad \text{(C2)}$$

In the limit, for $R\to\infty$, μ_p goes to μ_b. Therefore, the chemical potential of the bulk fluid is

$$\mu_b=\beta^{-1}\ln\frac{\rho_b\Lambda^3}{1-\rho_b b_b}+\beta^{-1}\frac{\rho_b b_b}{1-\rho_b b_b}-2a_b\rho_b\frac{C\epsilon^{\mathrm{HB}}}{2}\left\{\left(\sum_{j=1}^{4} jp_j^b+\sum_{j=5}^{7}(8-j)p_j^b\right)+\rho_b\left(\sum_{j=1}^{4} j\frac{\partial p_j^b}{\partial\rho_b}+\sum_{j=5}^{7}(8-j)\frac{\partial p_j^b}{\partial\rho_b}\right)\right\}. \quad \text{(C3)}$$

[1] A. Giaya, R. W. Thompson, and R. Denkewicz, Microporous Mesoporous Mater. **40**, 205 (2000).
[2] A. Giaya and R. W. Thompson, Microporous Mesoporous Mater. (unpublished).
[3] S. J. Gregg and K. S. W. Sing, *Adsorption, Surface Area and Porosity*, 2nd ed. (Academic, London, 1982).
[4] A. Kohlmeyer, C. Hartnig, and E. Spohr, J. Mol. Liq. **78**, 233 (1998).
[5] D. Diestler and M. Schoen, Acta Chim. Hung. **132**, 45 (1995).
[6] M. Schoen and D. Diestler, J. Chem. Phys. **109**, 5596 (1998).
[7] T. M. Truskett, P. G. Debenedetti, and S. Torquato, J. Chem. Phys. **114**, 2401 (2001).
[8] T. M. Truskett, P. G. Debenedetti, S. Sastry, and S. Torquato, J. Chem. Phys. **111**, 2647 (1999).
[9] A. Giaya and R. W. Thompson, J. Chem. Phys. **116**, 2565 (2002).
[10] C. Garrod, *Statistical Mechanics and Thermodynamics* (Oxford University Press, New York, 1995).
[11] P. Jedlovszky, J. P. Brodholt, F. Bruni, M. A. Ricci, A. K. Soper, and R. Vallauri, J. Chem. Phys. **108**, 8528 (1998).
[12] K. A. Silverstein, A. Haymet, and K. A. Dill, J. Am. Chem. Soc. **122**, 8037 (2000).
[13] S. Torquato, Phys. Rev. E **51**, 3170 (1995).
[14] M. Rovere, M. Ricci, D. Vellati, and F. Bruni, J. Chem. Phys. **108**, 9859 (1998).
[15] P. Atkins, *Physical Chemistry*, 6th ed. (Freeman, New York, 1998).
[16] J. A. Dean, *Lange's Handbook of Chemistry*, 14th ed. (McGraw–Hill, New York, 1992).
[17] K. Lum, D. Chandler, and J. D. Weeks, J. Phys. Chem. B **103**, 4570 (1999).
[18] M. W. Anderson and J. Klinowski, J. Chem. Soc., Faraday Trans. 1 **82**, 1449 (1986).
[19] J. Weitkamp, P. Kleinschmit, A. Kiss, and C. H. Berke, in *Proceedings of the Ninth International Zeolite Conference*, edited by R. von Ballmos, J. B. Higgins, and M. M. J. Treacy (Butterworth–Heinemann, Stoneham, MA, 1993), p. 79.
[20] D. Olson, W. Haag, and W. Borghard, Microporous Mesoporous Mater **35**, 435 (2000).
[21] E. M. Flanigen, J. M. Bennett, and R. Grose, Nature (London) **271**, 512 (1978).